DOI: 10.1002/ejoc.200800146

Helical Porphyrinoids: Incorporation of Ferrocene Subunits into Macrocyclic Structures

Marcin Stępień,[a] Irena Simkowa,[a] and Lechosław Latos-Grażyński*[a]

Keywords: Porphyrinoids / Metallocenes / NMR spectroscopy / Conformational analysis

Ferrocene-containing porphyrinoids have been synthesized in which ferrocene-1,1′-diyl units are linked to a dipyrrin or thiatripyrrin to form macrocyclic structures. NMR spectroscopic evidence shows that these new systems adopt helical conformations that undergo an inversion process in solution. In addition, small amounts of unexpected scrambling products have been isolated and characterized, namely a dipyrrin-bisferrocenophane and two expanded bis(ferrocene) macrocycles. The formation of these systems, which contain macrocyclic rings of different sizes, is a consequence of the structural flexibility of the ferrocene unit. Cyclic voltammetry shows that ferrocene oxidation is reversible in all the systems reported here, and that it is finely tuned by the properties of the ring system.

Introduction

Molecular structures with well-defined helicity are of particular theoretical and practical importance to chemistry.[1] The interest in helical structures stems in part from the occurrence of screw-like motifs in important biomolecules, such as proteins, nucleic acids, or polysaccharides, and the self-assembly of helical superstructures observed in these systems has been mimicked in a variety of artificial supramolecules.[2–6] Alternatively, molecular helicity may result from an appropriate design of a covalent structure, best exemplified by the syntheses of numerous aromatic helicenes.[1,7]

In porphyrinoid chemistry, helical structures are a consequence of macrocycle expansion[8–15] or occur in sterically congested noncyclic oligopyrroles, such as biliverdins.[16] In the case of expanded porphyrins, the helicity is associated with twisted, figure-of-eight structures,[8–15] some of which are stable enough to be separated into enantiomers.[11] Helical conformations of biliverdins and related conjugated oligopyrroles are involved in complex conformational equilibria,[16] but can be stabilized by additional bridging[17,18] or metal coordination. In particular, iron biliverdins (**1**), which are important intermediates in heme degradation, possess helical structures both in the solid state[19,20] and inside the active site of heme oxygenase.[21]

Metallocene units possessing rotational freedom around the main axis have been used as flexible "helicity elements," for example, in *ansa*-bridged systems[22] and ferrocene-containing peptides.[23,24] Importantly, the helical structure of some metallocene-based polymerization catalysts is the basis of their high stereoselectivity.[25,26] A particularly striking example of a helical ferrocene derivative is provided by the helicene complex **2**, first reported by Katz and coworkers.[27,28] This system, in which the iron atom is bound by a single fully π-conjugated ligand, demonstrates a structural paradigm that can potentially be extended to porphyrinoid chemistry. Specifically, one can envisage molecules of the general structure **3** (Scheme 1) which combine biliverdin-type helicity with that of 1,1′-disubstituted ferrocene. Such structures, if they possess at least partial conjugation in the oligopyrrole bridge, will belong to the large family of porphyrin analogues that contain carbo- and heterocyclic rings in place of pyrrole.[29–34]

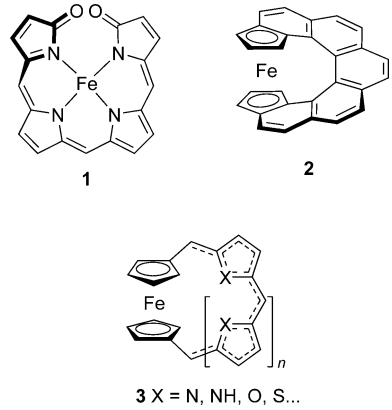

Scheme 1.

To date, metallocene subunits have chiefly been used as electroactive substituents or linkers in single- and multiporphyrin structures,[35–40] but have seldom constituted an

[a] Uniwersytet Wrocławski,
ul. F. Joliot-Curie 14, 50-383 Wrocław, Poland
Fax: +48-71-3282348
E-mail: llg@wchuwr.pl
Supporting information for this article is available on the WWW under http://www.eurjoc.org or from the author.

integral part of the macrocycle. In 1998, Sessler and coworkers reported *ansa*-bridged ferrocene macrocycles **4** which contain a ferrocene-1,1′-diyl unit and two pyrrole rings strapped together with an amide-linked oligoether or alkane chain.[41,42] These anion receptors were tested as electrochemical sensors for fluoride and dihydrogen phosphate. The ferrocene-1,1′-diyl building block was recently reemployed by Ramakrishnan and Srinivasan who prepared a series of calixpyrrole-ferrocene hybrids of the general structure **5** (Scheme 2).[43] In both **4** and **5**, the *ansa* bridge is not conjugated and only contains isolated pyrrole rings. Herein we report the first *ansa*-ferrocene macrocycles in which the metallocene sandwich is strapped together with a conjugated oligopyrrole unit, such as a dipyrrin or heterotripyrrin. The helical conformations of these macrocycles and their dynamic behavior have been explored by NMR spectroscopy.

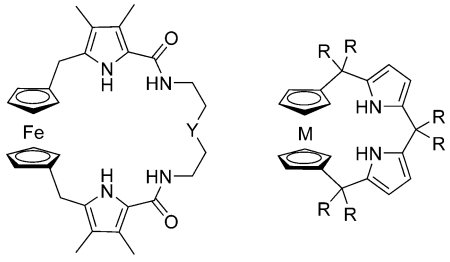

4a X = -OCH_2CH_2O-
4b X = -O-
4c X = -CH_2-

M = Fe, Ru
5

Scheme 2.

Results and Discussion

Nomenclature

Systems that incorporate the ferrocene-1,1′-diyl moiety, such as **4** or **5**, can be viewed as organometallic iron(II) complexes of linear, pyrrole-containing ligands in which the metal ion acts as a buckle fastening the ends of an organic "belt." Such an alternative description, although being apparently more complex, offers several practical advantages. For ligands comprising five-membered rings and *meso* bridges, it provides a formal link to typical oligopyrrole structures. Consequently, it can be used to develop a general nomenclature system and a numbering scheme for a large family of macrocycles. This naming system is described below (Scheme 3).

When the two NH groups in the terminal pyrrole rings of bilane are replaced with CH_2 units, one obtains a structure that can be simply termed 21,24-dicarbabilane, in accordance with the convention adopted in porphyrinoid chemistry.[29] (Note that the numbering of linear tetrapyrroles, such as bilane, traditionally omits position 20, which pertains to the "missing" *meso* carbon). According to general organometallic nomenclature, the ferrocene-like Fe^{II} complex of 21,24-dicarbabilane can then be named 1–4,16–19,21,24η-21,24-dicarbabilane-21,24-diyl iron(II), with the

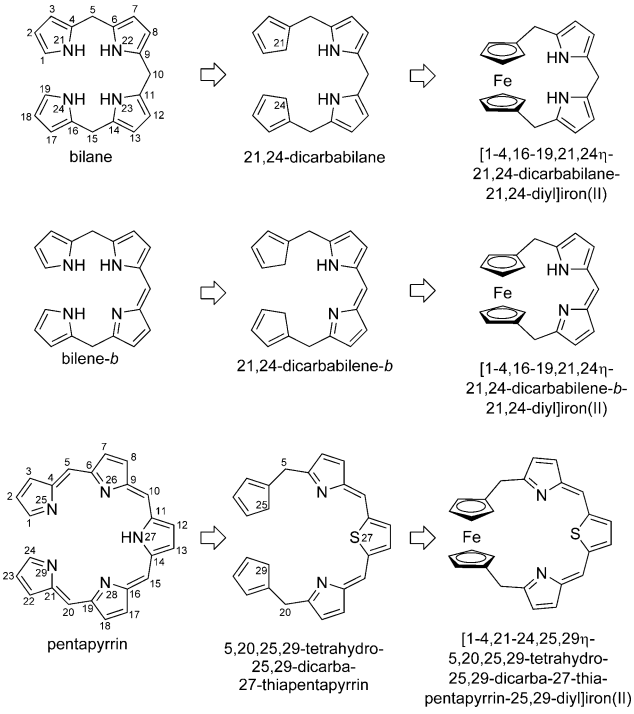

Scheme 3. Proposed nomenclature of ferrocene-based porphyrinoids.

initial sequence of locants indicating the binding mode of Fe^{II}. The same method can be applied to the naming of related systems derived from partly conjugated tetrapyrroles, such as bilene-*b*, as well as from longer oligopyrroles, for example, pentapyrrins (Scheme 3). The system proposed here can easily accommodate ligands of different chain lengths, oxidation levels, and substitution patterns.

Synthesis

Two distinct synthetic strategies can be used for the construction of ferrocene-containing macrocycles. In the first one, used by Sessler et al. in the synthesis of **4**, the organic ligand is constructed first, at least up to a certain point, before assembling the ferrocene unit.[41] In an alternative approach, employed in the preparation of **5**, unsubstituted ferrocene is used as the initial substrate, and is subsequently derivatized to yield the desired macrocyclic structure.[43] The latter method was independently pursued in our laboratory, yielding a number of new porphyrinoids with varying ring sizes and oxidation levels. The synthetic work is summarized in Scheme 4.

The linear substrate **6**, from which all the macrocyclic products were obtained, was prepared from ferrocene, acetone, and pyrrole in a simple, three-step procedure, which was essentially identical to the method reported by Ramakrishnan and Srinivasan.[43] The reactivity of **6** was initially tested by subjecting it to acid-catalyzed condensation reactions with aromatic aldehydes, followed by stoichiometric oxidation with 3,4-dichloro-5,6-dicyano-1,4-benzoquinone (DDQ). In both cases studied, the expected dicarbabilene-

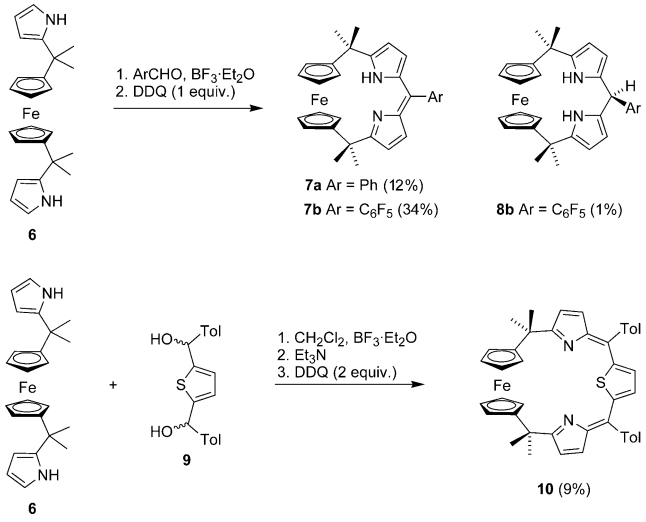

Scheme 4.

b derivative **7** was indeed formed as the main product. In addition, we were able to isolate and characterize small amounts of other ferrocene macrocycles, including the dicarbabilane complex **8b** (Scheme 4). The structures of all the compounds were elucidated with the aid of one- and two-dimensional NMR spectroscopy and high-resolution mass spectrometry, as discussed in detail below.

Having shown that **6** can be effectively used to construct porphyrinoid macrocycles, we attempted to prepare a system with an increased conjugation length in the oligopyrrolic fragment. Accordingly, compound **6** was treated with thiophene dicarbinol **9** to afford the expanded macrocycle **10** in 9% yield. This system can be viewed as a calixphyrin analogue containing one thiophene ring and one ferrocene-1,1′-diyl moiety.

Dicarbabilene-*b* Complexes 7a and 7b

Iron(II) dicarbabilene-*b*-diyls **7a** and **7b** were purified by column chromatography and isolated as bright-orange compounds with excellent solubility in most organic solvents and a poor tendency to crystallize. The structural information needed to confirm the identity of the compounds was therefore drawn from one- and two-dimensional NMR spectroscopy.

The ^{1}H NMR spectrum of **7a**, recorded in [D]chloroform at 298 K, shows features common to both dicarbabilene-*b* derivatives (Figure 1). Two coupled signals corresponding to β-pyrrolic protons are observed at δ = 6.61 and 6.28 ppm. Each of these signals showed an additional coupling to a signal located at a much lower field (δ = 15.73 ppm) which was therefore assigned to the inner NH proton. The symmetry of the spectrum indicates that this proton is rapidly transferred between the two nitrogen atoms in a degenerate tautomeric process similar to that observed in simple dipyrrins[44] and porphodimethenes (e.g., see ref.[36]). Importantly, the marked downfield shift of the inner NH signal and its relative sharpness are indicative of strong intramolecular hydrogen bonding, which is presumably enhanced by the compression of the N···N distance induced by the relatively small size of the macrocycle in **7**. For comparison, the NH resonance of 5-phenyldipyrrin is observed as an extremely broad line centered at δ = 12.5 ppm,[44] whereas the corresponding resonance in a ferrocenyl-substituted porphodimethene is located at 12.8 ppm.[36]

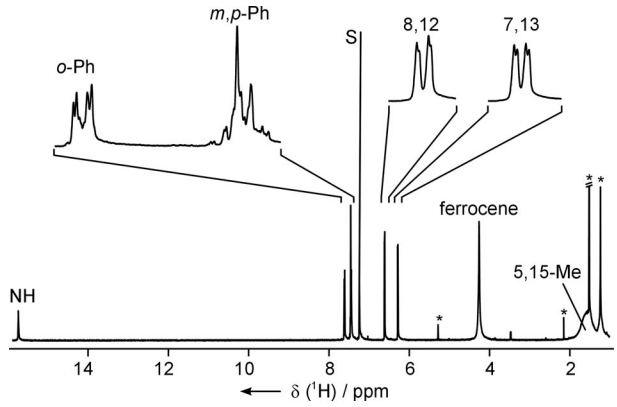

Figure 1. ^{1}H NMR spectrum of **7a** (500 MHz, $CDCl_3$, 298 K). The atom numbering follows that given in Scheme 3.

Further inspection of the room-temperature ^{1}H NMR spectra of **7a** and **7b** reveals significant dynamic broadening of the signals corresponding to the ferrocene moiety (ca. 4.3 ppm) and *meso*-methyl groups (ca. 1.6 ppm). The dynamic process responsible for the broadening can be frozen out by lowering the temperature, the slow exchange limit being more easily accessible for **7b** (Figure 2). In the ^{1}H NMR spectrum of **7b** obtained at 253 K, four distinct signals are present in the ferrocene region, whereas in the *meso*-methyl region, two resonances are observed. Thus in the slow exchange limit, the spectrum of **7b** is consistent with an effective C_2 point symmetry, which is in agreement with the chiral conformation predicted for **7b** by semi-empirical calculations (Figure 3).

The calculated geometry is in good qualitative agreement with the results of a preliminary X-ray structural determination of **7a** (see the Supporting Information). The helical twist of the dicarbabilene-*b* ligand in **7b** results in the nonequivalence of the methyl groups on each *meso* bridge and differentiation of the four protons on each face of the ferrocene subunit. At higher temperatures the helix untwists rapidly, leading to fast exchange between the enantiomeric configurations *M* and *P* (Figure 3). In the fast exchange limit, two ferrocene signals and one methyl signal are observed, in agreement with an effective C_{2v} symmetry of the molecule.

Note that in the variable-temperature NMR spectra of **7b**, the positions of peaks observed in the fast exchange limit do not coincide with the averaged shifts of exchanging protons observed in slow exchange. This observation can be

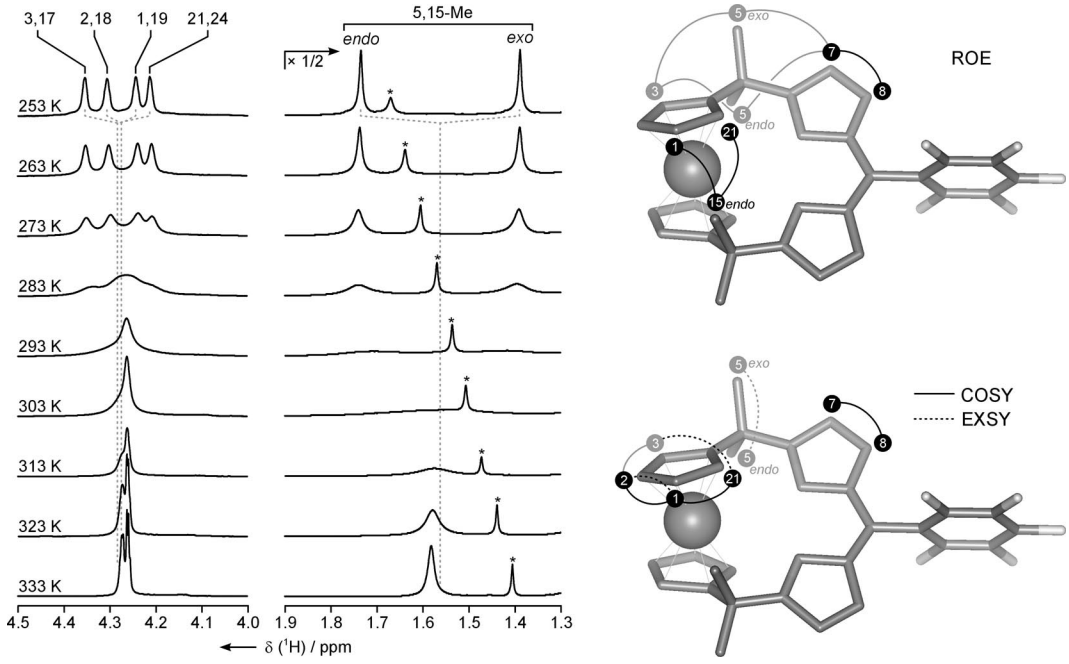

Figure 2. Partial ^{1}H NMR spectrum of **7b** showing the temperature dependence of the ferrocene and methyl regions (500 MHz, CD_2Cl_2, 333–253 K, left). Signals were assigned on the basis of 2D NMR spectroscopy (COSY, ROESY, 253 K). The connectivities used for the assignment are overlaid on a calculated geometry of **7b** (PM3/RHF, right).

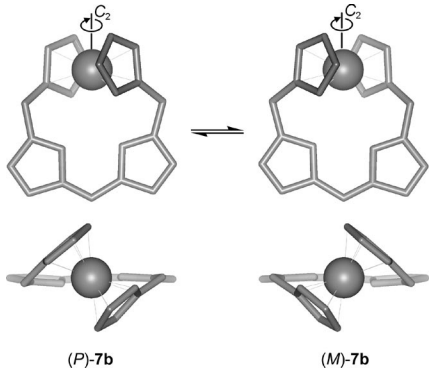

Figure 3. Helix inversion in **7b**. The model shown was obtained from semi-empirical calculations (PM3/RHF). The iron atom is represented as a sphere. Hydrogen atoms and substituents have been omitted for clarity.

interpreted as a solvent effect, but it may also indicate that helix inversion proceeds with the intermediacy of an additional conformer of unspecified geometry whose population varies with temperature. Nevertheless, quantitative analysis of the line-broadening was attempted in order to obtain estimates of the activation parameters for helix inversion in **7a** and **7b** (Table 1). In both cases, inversion rates were fitted to the Eyring equation, showing a satisfactory linear dependence on $1/T$. Both systems have similar activation enthalpies of approximately 70 kJ/mol, whereas the entropy value $\Delta S^{\ddagger}$ is noticeably lower for **7b**. However, the above values may not have a simple physical meaning as they would likely be affected by a pre-equilibrium involving the putative intermediate conformer.

Table 1. Physical data for ferrocene porphyrinoids.

	$\Delta H^{\ddagger}$[a] [kJ/mol]	$\Delta S^{\ddagger}$[a] [J/mol K]	$\Delta G^{\ddagger}$[a,b] [kJ/mol]	ω[c] [°]	Θ[c] [°]
7a	70.5(1.5)	55.9(5.6)	53.9(3.1)	107.4	13.4
7b	67.9(1.2)	38.4(4.3)	56.4(2.5)	107.4	13.4
8b	103.8(1.5)	106.5(4.7)	72.1(2.9)	95.4	8.6
10	71.6(1.9)	43.2(6.8)	58.7(3.9)	153.3	1.7

[a] Activation parameters for helix inversion calculated from the Eyring equation (error estimates are given in parentheses). [b] At 298 K. [c] Parameters were calculated from the PM3 models. For definitions see the text.

The electronic spectrum of **7b** recorded in *n*-hexane (Figure 4) is quite similar to the spectrum of 5-phenyldipyrrin,[44] both in appearance and intensity. The ferrocene ab-

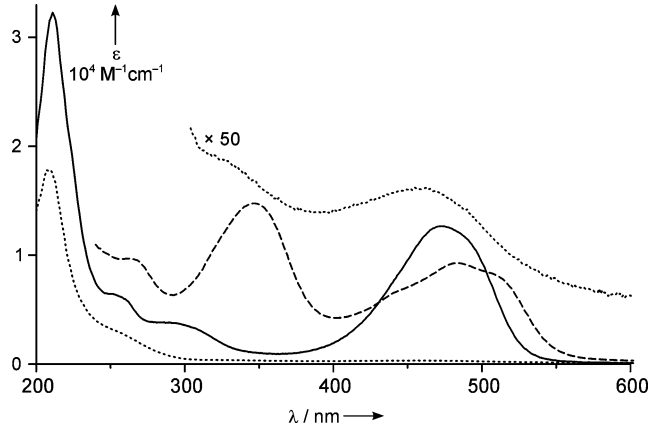

Figure 4. Electronic absorption spectra of **7b** (*n*-hexane, 298 K, solid line), **8b** (*n*-hexane, 298 K, dotted line), and **10** (CH_2Cl_2, 298 K, dashed line).

sorption in the visible range is relatively weak ($\log\varepsilon \approx 2$)[45] and is therefore overshadowed by the more intense absorption of the dipyrrin fragment ($\log\varepsilon \approx 4$).

Dicarbabilane Complex 8b

Compound **8b** was initially isolated as one of the byproducts in the synthesis of **7b** (Scheme 4). It can be obtained directly in the condensation of **6** and pentafluorobenzaldehyde when the oxidation step is omitted. Compound **8b** has limited stability in the presence of atmospheric oxygen and undergoes slow oxidation to **7b**. The strong dipyrrin absorption is absent from the electronic spectrum of **8b** and the weak coloring of this compound is solely due to the absorption band of ferrocene (Figure 4).

The ^{1}H NMR spectrum of **8b** recorded at 273 K (Figure 5) displays four β-pyrrolic and eight ferrocene resonances, corresponding to a structure of the lowest symmetry (C_1). At higher temperatures, the signals experience dynamic broadening similar to that observed for **7a**,**b**. This behavior strongly suggests that **8b** also adopts a helical conformation which is similarly involved in an inversion process. However, the unsymmetrical substitution at C-10 lowers the observed symmetry of the NMR spectrum both in the slow and fast exchange limit (C_1 and C_s, respectively).

Complete assignment of all the signals was achieved through a combination of homonuclear correlation techniques (COSY, NOESY, ROESY). The resulting structural information derived from 2D NMR spectra is consistent with the conformation of **8b** obtained from semi-empirical calculations (Figure 5). In the first step of the analysis, scalar couplings observed in the COSY map were used to distinguish spin systems of the pyrrole and cyclopentadienyl rings (^3J and ^4J couplings) and to identify the signals of methyl groups attached to a single *meso*-carbon atom (^4J couplings). EXSY-type correlations observed in the NOESY and ROESY spectra were subsequently employed to pair signals of exchanging protons in the molecule. The helix inversion process swaps the two halves of the dicarbabilane ligand to create exchange correlations between 8-H and 12-H, 7-H and 13-H, etc. (Figure 6). Interestingly, the conformational change associated with the inversion causes the *endo*-5-Me and -15-Me groups to exchange with the *exo*-15-Me and -5-Me groups, respectively. Dipolar couplings observed in the NOESY and ROESY spectra provide information on the spatial relationships of the different fragments of the molecule. In particular, they helped establish the adjacency of particular structural elements in the dicarbabilane framework. A number of additional contacts were identified between the *endo*-methyl groups and selected cyclopentadienyl (Cp) protons of the opposite half of the ligand, which indicates that it is indeed folded into a macrocyclic structure.

An unresolved problem that remained was that of assigning the two nonequivalent sets of peaks to specific halves of the molecule. This apparently difficult question could be answered by interpreting the benzylic ^4J coupling observed between the *meso*-proton (10-H) and only one of the neighboring β-pyrrolic protons (either 8-H or 12-H). The benzylic coupling is known to linearly depend on π bond order (the same for both pyrroles) and to have a $\sin^2\theta$ dependence on the torsional angle θ between the aromatic and the C–H bonds.[46] The latter relationship gives a maximum for the perpendicular orientation of the two bonds, for which the overlap between the C–H bond and the π density is most efficient. In the PM3 model of **8b**, the torsional angles C8–C9–C10–H10 and C12–C11–C10–H10 are equal to –124 and 23°, respectively (the signs correspond to

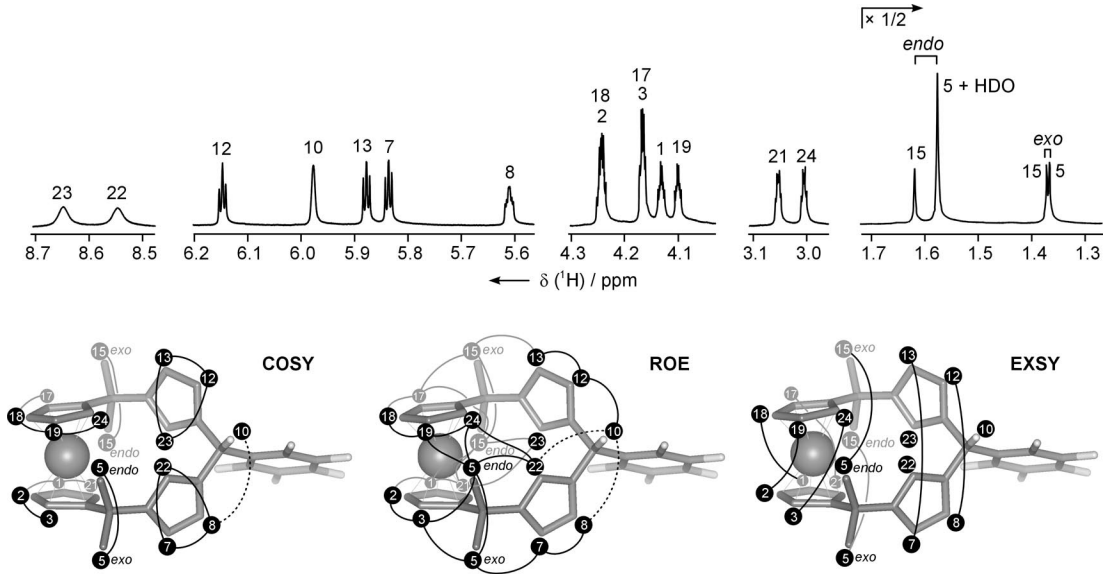

Figure 5. ^{1}H NMR spectrum of **8b** (top, 500 MHz, $CDCl_3$, 273 K). The numbering scheme corresponds to that given in Scheme 3. The conformation of **8b** was obtained from molecular modeling (PM3/RHF). The iron atom is represented as a sphere. Hydrogen atoms (with the exception of 10-H) have been omitted for clarity. The connectivities shown in the bottom panels were obtained from COSY (273 K, left), ROESY (223 K, center), and ROESY (298 K, right) spectra. Dotted lines denote weak couplings.

the enantiomer shown in Figure 6). Thus, as assumed in the proposed assignment, 8-H should be the one more strongly coupled to 10-H.

In macrocyclic structures such as **7** or **8**, the rotational freedom of the Cp rings, a characteristic of unsubstituted ferrocene, is restricted by the *ansa* bridge. The length of the bridge will affect the relative orientation of the substituted carbon atoms (1 and 1′) of the two Cp rings. This orientation can be parametrized with a torsional angle ω, defined by the sequence C1–Ct–Ct′–C1′, where C1 and C1′ are the substituted carbon atoms of the ferrocene-1,1′-diyl group and Ct and Ct′ denote the centroids of the respective Cp rings.[23,24] The ω parameter takes a value of 107 and 95° for the calculated geometries of **7a** and **8b**, respectively (Table 1). These values are in good agreement with the ω angle measured in the solid-state structure of a related dicarbabilane macrocycle (112°).[43] On the other hand, the angle θ between the Cp rings[23] is estimated to be 13° in **7a**,**b** and 9° in **8b**, which indicates a slight distortion of ferrocene from coplanarity which is caused by *ansa* bridging.

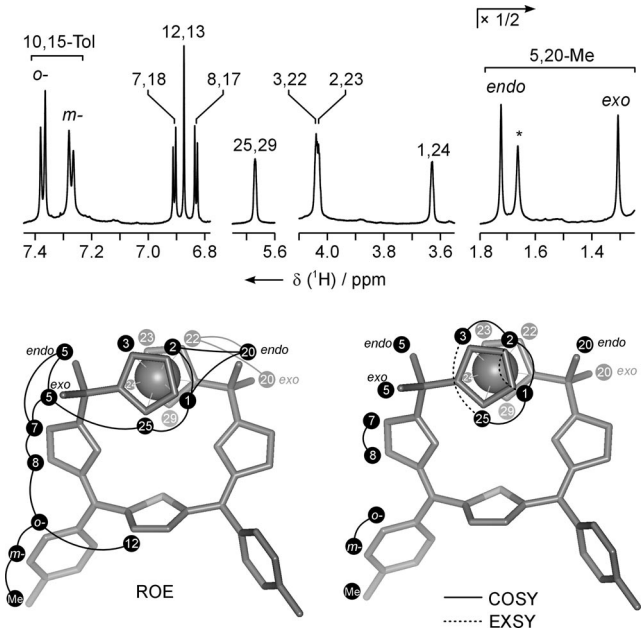

Figure 6. ^{1}H NMR spectrum of **10** (top, 500 MHz, CD_2Cl_2, 233 K). The numbering scheme corresponds to that given in Scheme 3. The connectivities shown in the bottom panels were obtained from ROESY (233 K, left), COSY (233 K, right, solid lines), and ROESY (exchange peaks at 233 K, right, dotted lines) spectra. The conformation of **10** shown in the figure was obtained from semi-empirical calculations (PM3/RHF).

Macrocycle 10

In the porphyrinoid macrocycles described above, the inner cavity is relatively small and congested. The synthesis of **10** was therefore attempted with the goal of creating a more porphyrin-like structure which would possess more extensive π conjugation and, potentially, an ability to bind metal ions. Compound **10** proved very difficult to isolate and characterize and our initial preparative efforts did not give consistent results. It was eventually found that **10** undergoes partial one-electron oxidation during work-up, a process that could not be completely avoided even in an inert atmosphere. The amount of the resulting ferrocenium species formed increased with each additional purification step, leading to substantial broadening of the ^{1}H NMR spectrum of **10** which was caused by exchange with the paramagnetic cation. It was ultimately discovered that the most expedient way to deal with this broadening was to add a small amount of zinc amalgam to the NMR sample, thus effectively removing the paramagnetic admixture.

The ^{1}H NMR spectrum of **10**, recorded at 233 K, corresponds to a structure with two-fold symmetry (Figure 6). In particular, it contains four resonances in the range of 3.6–5.7 ppm, ascribable to the ferrocene fragment and two signals, at δ = 1.72 and 1.31 ppm, which have been assigned to *meso*-methyl substituents. The pattern of dipolar couplings obtained from the ROESY spectrum is consistent with the helical conformation shown in Figure 6, which was effectively modeled using semi-empirical methods (PM3/RHF). This helical structure bears a resemblance to the conformation proposed for **7**, except that in the case of **10**, the larger macrocyclic structure causes the ferrocene-1,1′-diyl unit to "open", which results in a much larger value of the ω parameter (153°). Additionally, the longer *ansa* bridge is predicted to impose relatively little strain on the ferrocene moiety, leading to a very small θ angle of around 2°.

Above 233 K, gradual broadening of the ferrocene and *meso*-Me signals is observed in the ^{1}H NMR spectrum of **10**. The exchange pattern observed in the ROESY spectrum at various temperatures strongly suggests that **10** undergoes a helix inversion process analogous to that postulated for the smaller macrocycles **7** and **8** (Figure 6). Note, however, that the variable-temperature NMR spectra of **10** reveal not only dynamic broadening, but also a marked temperature dependence of chemical shifts (see Figure S21 in the Supporting Information). The latter observation suggests that, in analogy to **7**, compound **10** may in fact possess several thermally accessible conformations that undergo fast exchange in a temperature-dependent equilibrium.

Characterization of Scrambling Products

Similarly to unconjugated oligopyrroles used in porphyrin chemistry, such as dipyrromethanes and tripyrranes, compound **6** is susceptible to "scrambling", that is, partial dissociation in the presence of an acid catalyst. This process is generally considered unfavorable in synthetic porphyrin chemistry as it is responsible for the formation of unwanted byproducts (e.g., isomers).[47] In the present case, the formation of scrambling products was of interest as it revealed an unexpected potential of the ferrocene-1,1′-diyl fragment to create macrocyclic structures of widely varying ring sizes. In particular, by scrutinizing the reaction mixtures obtained from the syntheses of **7a** and **7b**, we were able to isolate small amounts of three bis(ferrocene) compounds **11**–**13**

(Scheme 5) whose structures were elucidated by NMR spectroscopic methods and high-resolution mass spectrometry.

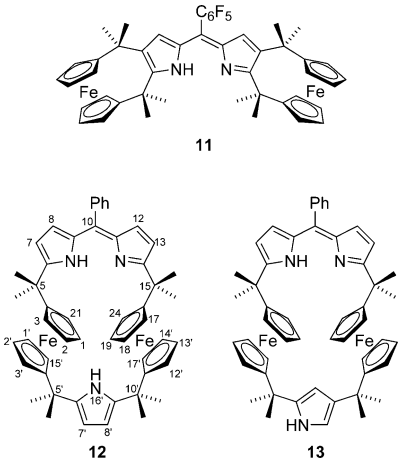

Scheme 5. Bis(ferrocene) products formed in the syntheses of **7a** and **7b**.

Compound **11**, obtained in trace amounts in the synthesis of **7b**, can be described as a dipyrrin derivative with two *ansa*-bridged ferrocenes attached to adjacent α and β positions of each pyrrole ring. We anticipate that such a structure may be of practical interest as it combines two electroactive ferrocene units with a chelating ligand known to form a variety of metal complexes, some of which are highly fluorescent.[48] Presumably, the formation of **11** begins with the acid-catalyzed dissociation of pyrrole from **6** (Scheme 6). The resulting carbocation **14** undergoes spontaneous ring closure through the β position of the remaining pyrrole ring to yield the pyrrole-ferrocenophane **15**. We suppose that in this step, the effect of proximity is responsible for overcoming the intrinsically lower reactivity of pyrrole β positions relative to the α positions. Two molecules of **15** then condense with the aldehyde and the resulting dipyrromethane is oxidized to **11**.

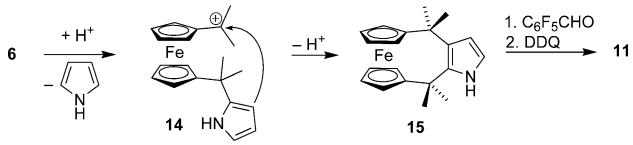

Scheme 6. Formation of compound **11**.

The spectroscopic data obtained for **11** are fully consistent with the proposed structure. The ^{1}H NMR spectrum, shown in Figure 7, reflects an overall C_{2v} symmetry of the molecule. The spectrum contains two pairs of ferrocene signals, corresponding to the nonequivalent Cp rings on each ferrocene unit. Additionally, the spectrum contains signals from two methyl groups, one resonance at δ = 6.32 ppm, which corresponds to the unsubstituted β-position (3,7-H), and a broad signal at δ = 12.30 ppm, assigned to the NH proton. The complete assignment of the resonances, based on correlation data, is shown in Figure 7.

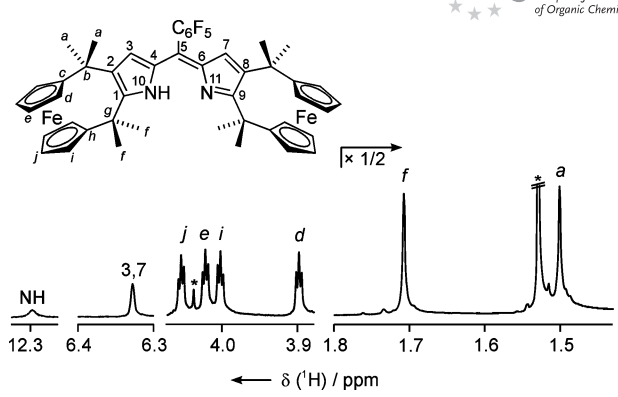

Figure 7. ^{1}H NMR spectrum of **11** (500 MHz, $CDCl_3$, 298 K). The labeling of the signals is explained in the inset.

By careful use of column chromatography, we were able to isolate two isomeric macrocycles **12** and **13** which were formed as byproducts in the synthesis of **7a**. To the best of our knowledge compounds **12** and **13**, each comprising three pyrrole rings and two ferrocene-1,1′-diyl units, are the largest ferrocene-based porphyrinoids reported to date. The two structures differ in the way the isolated pyrrole ring is incorporated into the structure. In compound **12**, the pyrrole is anchored in the standard way, that is, through its two α positions. Isomer **13** contains a pyrrole ring that is linked into the macrocycle through nonadjacent α and β positions. Such an anchoring mode, observed in various porphyrin analogues, is known as "N confusion".[30] In particular, N-confused isomers were observed to form spontaneously in the synthesis of porphyrins (à la Rothemund),[49,50] heteroporphyrins,[51,52] and calixpyrroles (à la Baeyer).[53] Alternatively, **12** and **13** can be viewed as binuclear iron(II) complexes with two bridging ligands. Specifically, **12** is composed of 21,24-dicarbabilene-*b* and 15,17-dicarbatripyrrane, whereas in **13**, the latter ligand is replaced with its N-confused variant, 7-aza-15,16,17-tricarbatripyrrane. The simplest mechanistic pathway that leads to **12** and **13** involves an initial condensation of two molecules of **6** with one molecule of benzaldehyde, followed by dissociation of one of the terminal pyrrole rings. In the last condensation step, the macrocycle is closed via the α position or one of the β positions, yielding after oxidation compound **12** or **13**, respectively.

The ^{1}H NMR spectrum of **13** is more complicated than the corresponding spectrum of **12** and the observed lowering of molecular symmetry in the former is a consequence of pyrrole N confusion (Figure 8). In particular, the spectrum of **13** contains eight ferrocene and four methyl signals, as opposed to the four and two signals, respectively, observed for **12**. Similar symmetry lowering is also observed in the pyrrole region and the signals of the N-confused ring of **13** can be clearly identified. Finally, each spectrum contains signals corresponding to a single phenyl substituent, one pyrrolic NH (7–8 ppm), and one dipyrrin NH (12–13 ppm). Further details of the signal assignment are given in the Supporting Information.

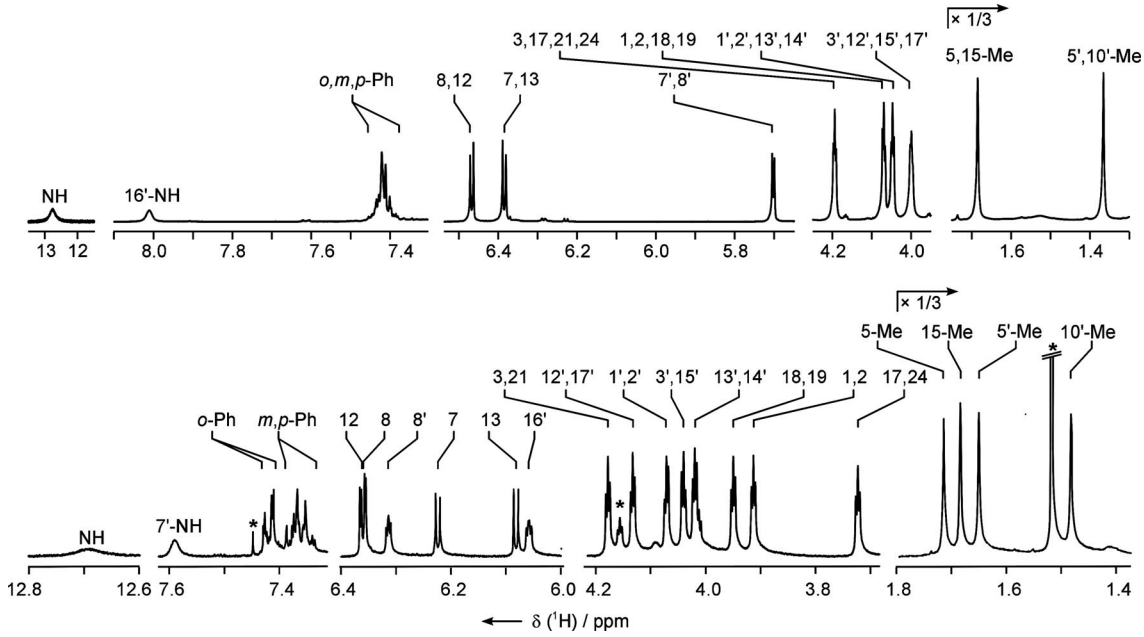

Figure 8. ^{1}H NMR spectra of **12** (top) and **13** (bottom, 500 MHz, $CDCl_3$, 298 K). The numbering scheme, given in Scheme 5, is identical for both structures. Details of the assignment are given in Figure S41 of the Supporting Information.

Electrochemistry

Cyclic voltammograms recorded for the dicarbabilene-*b* complexes **7a** and **7b** revealed two quasi-reversible oxidation processes and one reduction event (Table 2, Figure S42 of the Supplementary Information). The low-potential oxidation is easily identified as corresponding to the ferrocene unit and it is slightly cathodically shifted relative to the Fc^+/Fc couple (–0.06 and –0.04 V for **7a** and **7b**, respectively). The other two redox events correspond to the dipyrrin unit and accordingly exhibit a marked dependence on *meso* substitution. The more strongly electron-withdrawing C_6F_5 substituent in **7b** causes anodic shifts of the oxidation and reduction potentials (0.13 and 0.17 V, respectively) relative to those of the phenyl-substituted compound **7a**. On the other hand, the effect of the *meso* substituent on the ferrocene oxidation is very small. In compound **8b**, ferrocene oxidation can also be observed, but the features corresponding to the dipyrrin fragment are lost. Instead, only an irreversible wave at 0.79 V is observed, which is likely to be associated with the oxidation of **8b** to **7b**.

Ferrocene oxidation in compound **10** is shifted to –0.21 V relative to Fc/Fc^+, thus explaining the facile formation of a radical admixture during work-up. Additionally, there are two irreversible processes associated with the thiatripyrrane unit, namely an oxidation at around 1.03 V and a reduction at –1.45 V. As the inductive effects on the ferrocene caused by the attached *ansa* bridge should be comparable in **7** and **10**, the difference in the ferrocene oxidation potential between these two species may be tentatively interpreted as resulting from the different tilt of the Cp rings (measured by the θ angle).

Compounds **11**–**13** are structurally related in that each contains two ferrocene and one dipyrrin unit which are not π-conjugated and should therefore act as independent redox centers. Indeed, oxidation and reduction events corresponding to the dipyrrin fragment were identified in the cyclic voltammograms of all three systems **11**–**13** at potentials similar to those observed in **7a** and **7b**. However, in the bis(ferrocene) systems, dipyrrin oxidation and reduction showed much poorer reversibility. In compounds **11** and **12**, in which the two ferrocene subunits are structurally equivalent, a single oxidation wave of approximately doubled intensity was seen at 0.01 and –0.04 V, respectively, which indicates a very weak interaction between the metallocene units. On the other hand, in the cyclic voltammogram of **13**, two consecutive oxidations were observed in the ferrocene region at –0.12 and –0.01 V.

Table 2. Half-wave potentials (relative to Fc/Fc^+) for the ferrocene porphyrinoids.

	$E_{1/2}$ [V]			
7a	0.80	–0.06		–1.96
7b	0.93	–0.04		–1.79
8b	0.79[a]	0.01		
10	1.03[a]	–0.21		–1.45[a]
11	0.87	0.01		–2.01
12	0.88[a]	–0.04		–2.01[a]
13[b]	≈0.8[a]	–0.01	–0.12	–2.02[a]

[a] Irreversible. [b] An additional, less intense wave was observed at 0.17 V, which has been attributed to a ferrocene-containing impurity that could not be entirely removed from the samples of **13**.

Conclusions

Herein we have shown that the ferrocene-1,1′-diyl unit can be used as a versatile building block for the construc-

tion of new porphyrinoid molecules. A unique feature of this structural unit is its flexibility which results from the rotational freedom of the two cyclopentadienyl rings. As a result, a ferrocene-1,1′-diyl fragment can form macrocycles containing a varying number of heterocyclic units. To accommodate *ansa* bridges of different lengths, the two substituted Cp rings of ferrocene vary their relative orientation to yield helical structures such as **7** and **10**. The detection of small-ring pyrrole-ferrocenophanes (e.g., **11**) and expanded macrocycles (**12** and **13**), which form spontaneously as scrambling byproducts, provides a glimpse of the structural diversity available to ferrocene porphyrinoids.

The chemistry presented herein provides many opportunities for further study, such as the synthesis of systems with expanded macrocyclic cores, more extensive π conjugation, or precisely tuned redox properties. In addition, ferrocene-based porphyrinoids may be of significant interest as potential ligands, intriguingly allowing macrocyclic and metallocene coordination to be combined in close spatial proximity. Efforts to explore these various possibilities are ongoing in our laboratory.

Experimental Section

General: Unless noted otherwise, all reagents and solvents were used as received. Dichloromethane was distilled from calcium hydride. [D]Chloroform was deacidified by passing through a small alumina column. Compound **6** was obtained in a synthesis analogous to that described in ref.[43]. Compound **9** was obtained according to a literature procedure.[54] We thank Dr. Anna Berlicka who kindly provided the compound. Molecular models were obtained from semi-empirical calculations using the PM3 method in the restricted Hartree–Fock (RHF) mode, as implemented in HyperChem. 7.0. High-resolution mass spectra were recorded with a Micro ESI-Q-TOF spectrometer using electrospray ionization in the positive mode. In some cases DDQ was added to samples to improve ionization. Electrochemical measurements (CH_2Cl_2, 0.1 M TBAP) were performed with an EA9C Multifunctional Electrochemical Analyzer using a glassy-carbon working electrode, platinum wire as the auxiliary electrode, and silver wire as a reference electrode. The voltammograms were referenced against the half-wave potential of Fc/Fc^+.

NMR Spectroscopy: ^1H NMR spectra were recorded with a high-field spectrometer (Bruker Avance, ^1H frequency 500.13 MHz), equipped with a broad-band inverse-gradient probe head. Spectra were referenced to the residual solvent signals ([D]chloroform: δ = 7.24 ppm; [D_2]dichloromethane: δ = 5.32 ppm). Two-dimensional NMR spectra were recorded with 2048 data points in the t_2 domain and with up to 2048 points in the t_1 domain, with a 1 s recovery delay. All 2D NMR spectra were recorded with gradient selection with the exception of NOESY and ROESY spectra. The NOESY mixing time and ROESY spinlock time were 500 and 300 ms, respectively. ^{13}C NMR spectra were recorded with ^1H broadband decoupling and referenced to solvent signals ($^{13}CDCl_3$: δ = 77.0 ppm). ^1H–^{13}C correlation spectra are referenced to residual solvent signals ($^{13}CHCl_3$: δ_C = 77.2 ppm; $^{13}CHDCl_2$: δ_C = 54.0 ppm). Activation parameters for helix inversion were calculated using the Eyring equation. Rate constants were estimated from line-broadening of selected signals observed in the slow exchange limit ($k = \pi\nu_{1/2}$) and, where possible, in the fast exchange limit [$k = \pi\Delta\nu/(2\nu_{1/2})$].

Synthesis of 7a, 12, and 13: Compound **6** (271 mg, 0.90 mmol) and benzaldehyde (65 μL, 0.90 mmol) were dissolved in dichloromethane (600 mL) in a 1 L round-bottomed flask equipped with a stirring bar. The reaction mixture was purged with nitrogen for 20 min, after which time boron trifluoride–diethyl ether (60 μL) was added and the reaction was protected from light. After 2 h, triethylamine (68 μL) was added, followed by 3,4-dichloro-5,6-dicyano-1,4-benzoquionone (DDQ, 203 mg, 0.90 mmol). The solvent was removed on a rotary evaporator. Repeated column chromatography (grade II basic alumina, dichloromethane), monitored by NMR spectroscopy, enabled the isolation of **7a** and small amounts of **12** and **13** (ca. 1% each).

[1–4,16–19,21,24η-5,5,15,15-Tetramethyl-10-phenyl-21,24-dicarbabilene-*b*-21,24-diyl]iron(II) (7a): Orange solid; yield 54 mg (12%). ^1H NMR (500 MHz, $CDCl_3$, 298 K): δ = 15.73 (s, 1 H, NH), 7.61 (m, 2 H, *o*-Ph), 7.45 (m, 3 H, *m*,*p*-Ph), 6.61 (dd, ^3J = 4.1 Hz, 2 H, 8,12-H), 6.28 (dd, ^3J = 4.1 Hz, 2 H, 7,13-H), 4.26 (br., 8 H, 1,2,3,17,18,19,21,24-H), ca. 1.6 (br., 12 H, 5,5,15,15-Me) ppm. ^{13}C NMR (75 MHz, $CDCl_3$, 328 K): δ = 162.91, 140.35, 139.34, 137.10, 131.04, 128.91, 127.77, 127.38, 114.06, 114.00, 99.86, 67.50, 37.10, 32.25 ppm. HRMS (ESI+, DDQ added): calcd. for $C_{31}H_{30}FeN_2$ $[M]^+$ 486.1735; found 486.1758. UV/Vis (hexane): λ_{max} ($\log\varepsilon$) = 210 (4.55), 263 (3.83), 313 (3.82), 466 (4.09) nm.

[μ-{2(1–4,21η):1(16–19,24η)}5,5,15,15-Tetramethyl-10-phenyl-21,24-dicarbabilene-*b*-21,24-diyl][μ-{2(1–4,15η):1(11–14,17η)}-5,5,10,10-tetramethyl-15,17-dicarbatripyrrane-15,17-diyl]diiron (12): Orange solid; yield 4.2 mg (1%). ^1H NMR (500 MHz, $CDCl_3$, 298 K): δ = 12.76 (s, 1 H, NH), 8.01 (s, 1 H, 16′-NH), 7.46–7.38 (m, 5 H, *o*,*m*,*p*-Ph), 6.47 (d, ^3J = 4.2 Hz, 2 H, 8,12-H), 6.38 (d, ^3J = 4.2 Hz, 2 H, 7,13-H), 5.70 (d, ^3J = 2.7 Hz, 2 H, 7′,8′-H), 4.19 (m, 4 H, 3,17,21,24-H), 4.07 (m, 4 H, 1,2,18,19-H), 4.05 (m, 4 H, 1′,2′,13′,14′-H), 4.00 (m, 4 H, 3′,12′,15′,17′-H), 1.68 (s, 6 H, 5,15-Me), 1.37 (s, 6 H, 5′,10′-Me) ppm. ^{13}C NMR (126 MHz, $CDCl_3$, 298 K): δ = 163.53 (C-6,14), 139.40 (C-9,11), 138.89 (C-6′,9′), 137.67 (*i*-Ph), 130.64 (*o*-Ph), 128.38 (C-8,12), 128.30 (*p*-Ph), 127.42 (*m*-Ph), 116.37 (C-7,13), 101.70 (C-7′,8′), 100.15 (C-4′,11′), 99.02 (C-4,16), 68.03 (C-1′,2′,13′,14′), 67.93 (C-1,2,18,19), 66.08 (C-3′,12′,15′,17′), 66.02 (C-3,17,21,24), 36.61 (C-5,15), 34.15 (C-5′,10′), 30.39 (5′,10′-Me), 30.08 (5,15-Me) ppm. HRMS (ESI+): calcd. for $C_{51}H_{53}Fe_2N_3$ $[M - H]^+$ 819.2928; found 819.2938. UV/Vis (hexane): λ_{max} ($\log\varepsilon$) = 207 (4.53), 444 (3.95) nm.

[μ-{2(1–4,21η):1(16–19,24η)}5,5,15,15-Tetramethyl-10-phenyl-21,24-dicarbabilene-*b*-21,24-diyl][μ-{2(1–4,15η):1(11–14,17η)}-5,5,10,10-tetramethyl-7-aza-15,16,17-tricarbatripyrrane-15,17-diyl]-diiron (13): Orange solid; yield ca. 1%. ^1H NMR (500 MHz, $CDCl_3$, 298 K): δ = 12.69 (s, 1 H, NH), 7.59 (s, 1 H, 7′-NH), 7.42 (m, 2 H, *o*-Ph), 7.36, (m, 3 H, *m*,*p*-Ph), 6.36 (d, ^3J = 1.5 Hz, 1 H, 12-H), 6.35 (d, ^3J = 1.2 Hz, 1 H, 8-H), 6.31 (t, ^4J = 2.1 Hz, 1 H, 8′-H), 6.22 (d, ^3J = 4.1 Hz, 1 H, 7-H), 6.08 (d, ^3J = 4.3 Hz, 1 H, 13-H), 6.06 (t, ^4J = 2.1 Hz, 1 H, 6′-H), 4.18 (t, ^3J = 1.8 Hz, 2 H, 3,21-H), 4.13 (t, ^3J = 1.9 Hz, 2 H, 12′,17′-H), 4.07 (t, ^3J = 1.8 Hz, 2 H, 1′,2′-H), 4.04 (t, ^3J = 1.8 Hz, 2 H, 3′,15′-H), 4.02 (t, ^3J = 1.9 Hz, 2 H, 13′,14′-H), 3.95 (t, ^3J = 1.8 Hz, 2 H, 18,19-H), 3.92 (t, ^3J = 1.8 Hz, 2 H, 1,2-H), 1.71 (s, 6 H, 5-Me), 1.68 (s, 6 H, 15-Me), 1.65 (s, 6 H, 5′-Me), 1.48 (s, 6 H, 10′-Me) ppm. ^{13}C NMR (126 MHz, $CDCl_3$, 298 K, partial data extracted from 2D correlation spectra): δ = 168.7 (C-14), 160.0 (C-6), 140.1 (C-6′), 133.4 (C-9′), 130.6 (*o*-Ph), 130.1 (C-12), 128.2 (*p*-Ph), 127.3 (*m*-Ph), 126.2 (C-8), 117.4 (C-13), 114.0 (C-7), 111.4 (C-8′), 102.8 (C-16′), 102.5 (C-11′), 99.7 (C-4), 99.7 (C-4′), 98.2 (C-16), 68.3 (C-18,19), 68.2 (C-1,2), 67.7 (C-1′,2′), 67.3 (C-13′,14′), 67.0 (C-3,21), 66.9 (C-12′,17′), 66.7 (C-3′,15′), 66.3 (C-17,24), 36.4 (C-15), 36.1 (5-Me),

34.4 (C-5′), 33.5 (C-10′), 31.3 (10′-Me), 30.6 (5′-Me), 29.5 (5-Me), 28.1 (15-Me) ppm. HRMS (ESI+): calcd. for $C_{51}H_{54}Fe_2N_3$ $[M - H]^+$ 820.2987; found 820.3017. UV/Vis (hexane): λ_{max} ($\log\varepsilon$) = 207 (4.45), 307 (3.34), 445 (3.89) nm.

[1–4,16–19,21,24η-5,5,15,15-Tetramethyl-10-pentafluorophenyl-21,24-dicarbabilene-*b*-21,24-diyl]iron(II) (7b): Compound **7b** was prepared from **6** (302 mg, 0.75 mmol) and pentafluorobenzaldehyde (76 μL, 0.74 mmol) under conditions analogous to those used for the synthesis of **7a**. Column chromatography monitored by NMR spectroscopy afforded **7b** accompanied by smaller amounts of **8b** (1%) and **11** (< 1%). Yield 148 mg (34%). ^{1}H NMR (500 MHz, $CDCl_3$, 253 K): δ = 15.69 (s, 1 H, NH), 6.45 (d, ^3J = 3.8 Hz, 2 H, 8,12-H), 6.29 (dd, ^3J = 3.8, ^4J = 1.0 Hz, 2 H, 7,13-H), 4.35 (m, 2 H, 3,17-H), 4.31 (m, 2 H, 2,18-H), 4.24 (m, 2 H, 1,19-H), 4.21 (m, 2 H, 21,24-H), 1.74 (s, 6 H, 5,15-*endo*-Me), 1.40 (s, 6 H, 5,15-*exo*-Me) ppm. ^{13}C NMR (126 MHz, $CDCl_3$, 253 K, signals from the C_6F_5 substituent were not observed): δ = 164.00 (C-6,14), 138.43 (C-9,11), 125.40 (C-8,12), 115.15 (C-7,13), 98.82 (C-4,16), 69.98 (C-3,17), 67.79 (C-2,18), 67.03 (C-1,19), 65.18 (C-21,24), 36.95 (C-5,15), 32.11 (5,15-*endo*-Me), 31.56 (5,15-*exo*-Me) ppm. HRMS (ESI+): calcd. for $C_{31}H_{26}F_5FeN_2$ $[M - H]^+$ 577.1360; found 577.1366. UV/Vis (hexane): λ_{max} ($\log\varepsilon$) = 211 (4.51), 255 (3.80), 294 (3.58), 472 (4.10) nm.

[1–4,16–19,21,24η-5,5,15,15-Tetramethyl-10-petafluorophenyl-21,24-dicarbabilane-21,24-diyl]iron(II) (8b): Compound **8b** was prepared from **6** (159 mg, 0.52 mmol) and pentafluorobenzaldehyde (65 μL, 0.52 mmol) under conditions identical to those used for the synthesis of **7b**, except for the oxidation step, which was not included. Column chromatography afforded **8b** as a yellow-orange solid. Yield 90 mg (30%). ^{1}H NMR (500 MHz, $CDCl_3$, 273 K): δ = 8.65 (s, 1 H, 22-H), 8.56 (s, 1 H, 23-H), 6.15 (t, ^3J = 3.0 Hz, 1 H, 12-H), 5.98 (s, 1 H, 10-H), 5.88 (t, ^3J = 3.0 Hz, 1 H, 13-H), 5.84 (t, ^3J = 3.1 Hz, 1 H, 7-H), 5.61 (m, 1 H, 8-H), 4.24 (m, 2 H, 2, 18-H), 4.17 (m, 2 H, 3,17-H), 4.13 (m, 1 H, 1-H), 4.10 (m, 1 H, 19-H), 3.05 (m, 1 H, 21-H), 3.01 (m, 1 H, 24-H), 1.62 (s, 3 H, 15-*endo*-Me), 1.58 (s, 3 H, 5-*endo*-Me), 1.375 (s, 3 H, 15-*exo*-Me), 1.369 (s, 3 H, 5-*endo*-Me) ppm. ^{13}C NMR (126 MHz, $CDCl_3$, 298 K): δ = 145.00 (pseudo-d, $^1J_{CF}$ = 243 Hz, *o*/*m*-C_6F_5), 140.18 (pseudo-d, $^1J_{CF}$ = 253 Hz, *p*-C_6F_5), 139.01 (C-14), 138.30 (C-6), 137.72 (pseudo-dt, $^1J_{CF}$ = 252, J_{CF} = 16 Hz, *o*/*m*-C_6F_5), 126.83 (C-11), 125.62 (C-11/9), 116.84 (pseudo-t, J_{CF} = 17 Hz, *i*-C_6F_5), 108.44 (C-12), 105.93 (C-8), 104.49 (C-4), 104.43 (C-7), 104.28 (C-13), 103.38 (C-16), 68.41 (C-24), 67.98 (C-2/18), 67.97 (C-2/18), 67.86 (C-21), 66.81 (C-19), 66.71 (C-1), 65.27 (C-3/17), 65.13 (C-17/3), 34.36 (C-15), 34.30 (C-5), 32.77 (C-10), 31.53 (5-*endo*-Me), 30.86 (5-*exo*-Me), 30.82 (15-*exo*-Me), 19.90 (15-*endo*-Me) ppm. MS (ESI+): calcd. for $C_{31}H_{27}F_5FeN_2$ $[M]^+$ 578.2; found 578.1. UV/Vis (hexane): λ_{max} ($\log\varepsilon$) = 209 (4.25), 331 (2.16), 464 (2.53) nm.

[1,2,8,9-Tetrakis[2-(η^5-cyclopenta-1,3-diene-1,5-diyl)propan-2-yl]-5-pentafluoromethyldipyrrin]diiron (11): ^{1}H NMR (500 MHz, $CDCl_3$, 298 K, atom labeling is given in Figure 7): δ = 12.30 (s, 1 H, NH), 6.32 (s, 2 H, 3,7-H), 4.05 (pseudo-t, ^3J = 1.8 Hz, 4 H, *j*), 4.02 (pseudo-t, ^3J = 1.8 Hz, 4 H, *e*), 4.00 (pseudo-t, ^3J = 1.8 Hz, 4 H, *i*), 3.89 (pseudo-t, ^3J = 1.8 Hz, 4 H, *d*), 1.70 (s, 12 H, *f*), 1.50 (s, 12 H, *a*) ppm. ^{13}C NMR (126 MHz, $CDCl_3$, 298 K, atom labeling is given in Figure 7): δ = 162.15 (C-1,9), 140.76 (C-2,8), 134.62 (C-4,6), 125.06 (C-3,7), 118.89 (C-5), 98.25 (*c*), 95.84 (*h*), 67.84 (*e*), 67.72 (*j*), 65.97 (*i*), 65.84 (*d*), 37.86 (*g*), 34.72 (*b*), 33.66 (*a*), 32.37 (*f*) ppm. HRMS (ESI+): calcd. for $C_{47}H_{43}F_5Fe_2N_2$ $[M]^+$ 842.2010; found 842.2045.

[1–4,21–24,25,29η-10,15-Bis(*p*-tolyl)-5,5,20,20-tetramethyl-5,20,25,29-tetrahydro-25,29-dicarba-27-thiapentapyrrin-25,29-diyl]-iron (10): Compounds **6** (102 mg, 0.25 mmol) and **9** (82.2 mg, 0.25 mmol) were dissolved in dichloromethane (300 mL) in a 0.5 L round-bottomed flask equipped with a stirring bar and a nitrogen inlet. The reaction mixture was purged with nitrogen for 15 min, after which time boron trifluoride–diethyl ether (25 μL) was added and the mixture was protected from light and stirred for 2 h. Triethylamine (28 μL) was then added, followed by DDQ (115 mg, 0.5 mmol), and the resulting mixture was stripped of solvent on a rotary evaporator. The crude product was purified by chromatography in an inert atmosphere on a grade II basic alumina column using dichloromethane as the eluent. In the final purification step the product was converted into a tetrafluoroborate salt (by shaking a dichloromethane solution with dilute aqueous HBF_4). The acid salt was then precipitated from dichloromethane/hexane and filtered. The resulting solid was redissolved in dichloromethane and stirred with anhydrous potassium carbonate until full conversion to the free base was observed. The solution was then filtered and freed from solvent on a rotary evaporator, affording **10** as an orange solid. Yield 15.2 mg (9%) ^{1}H NMR (500 MHz, CD_2Cl_2, 233 K): δ = 7.37 (d, ^3J = 8.2 Hz, 4 H, *o*-Tol), 7.27 (d, ^3J = 8.2 Hz, 4 H, *m*-Tol), 6.91 (d, ^3J = 4.6 Hz, 2 H, 7,18-H), 6.87 (s, 2 H, 12,13-H), 6.83 (d, ^3J = 4.6 Hz, 2 H, 8,17-H), 5.67 (m, 2 H, 25,29-H), 4.04 (m, 2 H, 3,22-H), 4.03 (m, 2 H, 2,23-H), 3.63 (m, 2 H, 1,24-H), 2.42 (s, 3 H, Tol-Me), 1.72 (s, 3 H, 5,20-*endo*-Me), 1.31 (s, 3 H, 5,20-*exo*-Me) ppm. ^{13}C NMR (126 MHz, C_2DCl_2, 233 K, shifts extracted from 2D spectra): δ = 182.2 (C-6,19), 153.6 (C-9,16), 149.9 (C-11,14), 141.2 (C-10,15), 139.4 (*p*-Tol), 135.3 (C-8,17), 134.8 (*i*-Tol), 133.2 (C-12,13), 131.5 (*o*-Tol), 128.5 (*m*-Tol), 127.6 (C-7,18), 96.1 (C-4,21), 72.1 (C-25,29), 70.3 (C-1,24), 65.6 (C-2,23), 64.4 (C-3,22), 38.4 (C-5,20), 35.8 (5,20-*exo*-Me), 26.6 (5,20-*endo*-Me), 21.2 (Tol-Me) ppm. HRMS (ESI+): calcd. for $C_{44}H_{42}FeN_2S$ $[M - H]^+$ 685.2310; found 685.2340. UV/Vis (CH_2Cl_2, λ_{max} ($\log\varepsilon$) = 263 (3.99), 346 (4.17), 484 (3.98) nm.

Supporting Information (see also the footnote on the first page of this article): Additional figures and tables, containing 1D and 2D NMR spectra, high-resolution mass spectra, cyclic voltammograms, and dynamic NMR spectroscopic data are included.

Acknowledgments

Financial support from the the Ministry of Science and Higher Education (Grant PBZ-KBN-118/T09/2004) is kindly acknowledged.

[1] K. P. Meurer, F. Vögtle, *Top. Curr. Chem.* **1985**, *127*, 1.
[2] C. Piguet, G. Bernardinelli, G. Hopfgartner, *Chem. Rev.* **1997**, *97*, 2005.
[3] S. H. Gellman, *Acc. Chem. Res.* **1998**, *31*, 173.
[4] M. Albrecht, *Chem. Rev.* **2001**, *101*, 3457.
[5] J. R. Nitschke, *Acc. Chem. Res.* **2007**, *40*, 103.
[6] D. J. Hill, M. J. Mio, R. B. Prince, T. S. Hughes, J. S. Moore, *Chem. Rev.* **2001**, *101*, 3893.
[7] M. S. Newman, D. Lednicer, *J. Am. Chem. Soc.* **1956**, *78*, 4765.
[8] J. L. Sessler, S. J. Weghorn, V. Lynch, M. R. Johnson, *Angew. Chem. Int. Ed. Engl.* **1994**, *33*, 1509.
[9] E. Vogel, M. Bröring, J. Fink, D. Rosen, H. Schmickler, J. Lex, K. W. K. Chan, Y.-D. Wu, D. A. Plattner, M. Nendel, K. N. Houk, *Angew. Chem. Int. Ed. Engl.* **1995**, *34*, 2511.
[10] M. Bröring, J. Jendrny, L. Zander, H. Schmickler, J. Lex, Y.-D. Wu, M. Nendel, J. Chen, D. A. Plattner, K. N. Houk, E. Vogel, *Angew. Chem. Int. Ed. Engl.* **1995**, *34*, 2515.
[11] A. Werner, M. Michels, L. Zander, J. Lex, E. Vogel, *Angew. Chem. Int. Ed.* **1999**, *38*, 3650.
[12] J.-Y. Shin, H. Furuta, K. Yoza, S. Igarashi, A. Osuka, *J. Am. Chem. Soc.* **2001**, *123*, 7190.

[13] N. Sprutta, L. Latos-Grażyński, *Chem. Eur. J.* **2001**, *7*, 5099.
[14] H. Rath, J. Sankar, H. PrabhuRaja, T. K. Chandrashekar, B. S. Joshi, R. Roy, *Chem. Commun.* **2005**, 3343.
[15] M. Stępień, L. Latos-Grażyński, N. Sprutta, P. Chwalisz, L. Szterenberg, *Angew. Chem. Int. Ed.* **2007**, *46*, 7869.
[16] S. E. Braslavsky, A. R. Holzwarth, K. Schaffner, *Angew. Chem. Int. Ed. Engl.* **1983**, *22*, 656.
[17] D. Krois, H. Lehner, *J. Chem. Soc. Perkin Trans. 1* **1989**, 2179.
[18] D. Krois, H. Lehner, *Monatsh. Chem.* **1989**, *120*, 789.
[19] A. L. Balch, L. Latos-Grażyński, B. C. Noll, M. M. Olmstead, N. Safari, *J. Am. Chem. Soc.* **1993**, *115*, 9056.
[20] K. T. Nguyen, S. P. Rath, L. Latos-Grażyński, M. M. Olmstead, A. L. Balch, *J. Am. Chem. Soc.* **2004**, *126*, 6210.
[21] M. Sugishima, H. Sakamoto, Y. Higashimoto, M. Noguchi, K. Fukuyama, *J. Biol. Chem.* **2003**, *278*, 32352.
[22] R. L. Halterman, *Chem. Rev.* **1992**, *92*, 965.
[23] D. R. van Staveren, T. Weyhermüller, N. Metzler-Nolte, *Dalton Trans.* **2003**, 210.
[24] S. I. Kirin, H.-B. Kraatz, N. Metzler-Nolte, *Chem. Soc. Rev.* **2006**, *35*, 348.
[25] T. Nakano, Y. Okamoto, *Chem. Rev.* **2001**, *101*, 4013.
[26] P. Corradini, G. Guerra, L. Cavallo, *Acc. Chem. Res.* **2004**, *37*, 231.
[27] T. J. Katz, J. Pesti, *J. Am. Chem. Soc.* **1982**, *104*, 346.
[28] A. Sudhakar, T. J. Katz, *J. Am. Chem. Soc.* **1986**, *108*, 179.
[29] L. Latos-Grażyński, "Core Modified Heteroanalogues of Porphyrins and Metalloporphyrins" in *The Porphyrin Handbook* (Eds.: K. M. Kadish, K. M. Smith, R. Guilard), Academic Press, New York, **2000**, vol. 2, chapter 14, pp. 361–416.
[30] H. Maeda, H. Furuta, *Pure Appl. Chem.* **2006**, *78*, 29.
[31] M. Pawlicki, L. Latos-Grażyński, *Chem. Record* **2006**, *6*, 64.
[32] T. D. Lash, *Syntheses of Novel Porphyrinoid Chromophores* in *The Porphyrin Handbook* (Eds.: K. M. Kadish, K. M. Smith, R. Guilard), Academic Press, San Diego, **2000**, vol. 2, chapter 10, pp. 125–199.
[33] M. Stępień, L. Latos-Grażyński, *Acc. Chem. Res.* **2005**, *38*, 88.
[34] R. Myśliborski, L. Latos-Grażyński, L. Szterenberg, *Eur. J. Org. Chem.* **2006**, 3064.
[35] H. Imahori, H. Yamada, Y. Nishimura, I. Yamazaki, Y. Sakata, *J. Phys. Chem. B* **2000**, *104*, 2099.
[36] S. W. Rhee, Y. H. Na, Y. Do, J. Kim, *Inorg. Chim. Acta* **2000**, *309*, 49.
[37] D. T. Gryko, F. Zhao, A. A. Yasseri, K. M. Roth, D. F. Bocian, W. G. Kuhr, J. S. Lindsey, *J. Org. Chem.* **2000**, *65*, 7356.
[38] B. Koszarna, H. Butenschön, D. T. Gryko, *Org. Biomol. Chem.* **2005**, *3*, 2640.
[39] A. N. Cammidge, P. J. Scaife, G. Berber, D. L. Hughes, *Org. Lett.* **2005**, *7*, 3413.
[40] M. U. Winters, E. Dahlstedt, H. E. Blades, C. J. Wilson, M. J. Frampton, H. L. Anderson, B. Albinsson, *J. Am. Chem. Soc.* **2007**, *129*, 4291.
[41] M. Scherer, J. L. Sessler, A. Gebauer, V. Lynch, *Chem. Commun.* **1998**, 85.
[42] J. L. Sessler, R. S. Zimmerman, G. J. Kirkovits, A. Gebauer, M. Scherer, *J. Organomet. Chem.* **2001**, *637–639*, 343.
[43] S. Ramakrishnan, A. Srinivasan, *Org. Lett.* **2007**, ASAP.
[44] C. Brückner, V. Karunaratne, S. J. Rettig, D. Dolphin, *Can. J. Chem.* **1996**, *74*, 2182.
[45] A. T. Armstrong, F. Smith, E. Elder, S. P. McGlynn, *J. Chem. Phys.* **1967**, *46*, 4321.
[46] M. Barfield, C. J. Fallick, K. Hata, S. Sternhell, P. W. Westerman, *J. Am. Chem. Soc.* **1983**, *105*, 2178.
[47] B. J. Littler, Y. Ciringh, J. S. Lindsey, *J. Org. Chem.* **1999**, *64*, 2864.
[48] T. E. Wood, A. Thompson, *Chem. Rev.* **2007**, *107*, 1831.
[49] H. Furuta, T. Asano, T. Ogawa, *J. Am. Chem. Soc.* **1994**, *116*, 767.
[50] P. J. Chmielewski, L. Latos-Grażyński, K. Rachlewicz, T. Głowiak, *Angew. Chem. Int. Ed. Engl.* **1994**, *33*, 779.
[51] E. Pacholska, L. Latos-Grażyński, L. Szterenberg, Z. Ciunik, *J. Org. Chem.* **2000**, *65*, 8188.
[52] N. Sprutta, L. Latos-Grażyński, *Org. Lett.* **2001**, *3*, 1933.
[53] S. Depraetere, M. Smet, W. Dehaen, *Angew. Chem. Int. Ed.* **1999**, *38*, 3359.
[54] A. Ulman, J. Manassen, *J. Chem. Soc. Perkin Trans. 1* **1979**, 1066.

Received: February 6, 2008
Published Online: April 8, 2008

